

Relative Natural Gradient for Learning Large Complex Models

Ke Sun
 École Polytechnique
 sunk.edu@gmail.com

Frank Nielsen
 École Polytechnique
 Sony CSL
 Frank.Nielsen@acm.org

June 21, 2016

Abstract

Fisher information and natural gradient provided deep insights and powerful tools to artificial neural networks. However related analysis becomes more and more difficult as the learner's structure turns large and complex. This paper makes a preliminary step towards a new direction. We extract a local component of a large neuron system, and defines its relative Fisher information metric that describes accurately this small component, and is invariant to the other parts of the system. This concept is important because the geometry structure is much simplified and it can be easily applied to guide the learning of neural networks. We provide an analysis on a list of commonly used components, and demonstrate how to use this concept to further improve optimization.

1 Introduction

The Fisher Information Metric (FIM) $\mathcal{I}(\Theta) = (\mathcal{I}_{ij})$ of a statistical parametric model $p(\mathbf{x} | \Theta)$ of order D is defined by a $D \times D$ positive semidefinite (psd) matrix ($\mathcal{I}(\Theta) \succeq 0$) with coefficients

$$\mathcal{I}_{ij} = E_p \left[\frac{\partial l}{\partial \Theta_i} \frac{\partial l}{\partial \Theta_j} \right], \quad (1)$$

where $l(\Theta)$ denotes the log-likelihood function $\ln p(\mathbf{x} | \Theta)$. Under light regularity conditions, Equation (1) can be rewritten equivalently as

$$\mathcal{I}_{ij} = -E_p \left[\frac{\partial^2 l}{\partial \Theta_i \partial \Theta_j} \right] = 4 \int \frac{\partial \sqrt{p(\mathbf{x} | \Theta)}}{\partial \Theta_i} \frac{\partial \sqrt{p(\mathbf{x} | \Theta)}}{\partial \Theta_j} d\mathbf{x}. \quad (2)$$

For regular natural exponential families (NEFs) $l(\Theta) = \Theta^\top \mathbf{t}(\mathbf{x}) - F(\Theta)$ (log-linear models with sufficient statistics $\mathbf{t}(\mathbf{x})$), the FIM is $\mathcal{I}(\Theta) = \nabla^2 F(\Theta) \succ 0$, the Hessian of the moment generating function (mgf). Although exponential families can approximate arbitrarily *any* smooth density (Cobb et al., 1983), the mgf may not be available in closed-form nor computationally tractable (Montanari, 2015). Besides the fact that learning machines usually have often singularities (Watanabe, 2009) ($|\mathcal{I}(\Theta)| = 0$, not full rank) characterized by plateaux in gradient learning, computing/estimating the FIM of a large learning system is very challenging due to the *finiteness of data*, and the *large number* $\frac{D(D+1)}{2}$ of matrix coefficients to evaluate. Moreover,

gradient descent techniques require to invert this large matrix and to tune the learning rate. The FIM is *not* invariant and depends on the parameterization: $\mathcal{I}_{\Theta}(\Theta) = \mathbf{J}^T \mathcal{I}_{\Lambda}(\Lambda) \mathbf{J}$ where \mathbf{J} is the Jacobian matrix $J_{ij} = \frac{\partial \Lambda_i}{\partial \Theta_j}$. Therefore one may ponder whether we can always find a suitable parameterization that yields a diagonal FIM that is straightforward to invert. This fundamental problem of parameter orthogonalization was first investigated by Jeffreys (1961) for decorrelating the estimation of the *parameters of interest* from the *nuisance parameters*. Fisher diagonalization yields parameter orthogonalization (Cox and Reid, 1987), and prove useful when estimating $\hat{\Theta}$ using MLE that is asymptotically normally distributed, $\hat{\Theta}_n = G(\Theta, \mathcal{I}^{-1}(\Theta))/\sqrt{n}$, where $G(\theta_1, \theta_2)$ denotes a univariate or multivariate Gaussian distribution with mean θ_1 and variance θ_2 , and efficient since the variance of the estimator matches the Cramér-Rao lower bound. Using the chain rule of differentiation of calculus, this amounts to find a suitable parameterization $\Omega = \Omega(\Theta)$ satisfying

$$\sum_{i,j} E \left[\frac{\partial^2}{\partial \Theta_i \partial \Theta_j} \partial l(x; \theta) \right] \frac{\partial \Theta_i}{\partial \Omega_k} \frac{\partial \Theta_j}{\partial \Omega_l} = 0, \quad \forall k \neq l.$$

Thus in general, we end up with $\binom{D}{2} = \frac{D(D-1)}{2}$ (non-linear) partial differential equations to satisfy (Huzurbazar, 1950). Therefore, in general there is no solution when $\binom{D}{2} > D$, that is when $D > 3$. When $D = 2$, the single differential equations is usually solvable and tractable, and the solution may not be unique: For example, Huzurbazar (1950) reports two orthogonalization schemes for the location-scale families $\{\frac{1}{\sigma} p_0(\frac{x-\mu}{\sigma})\}$ that include the Gaussian family and the Cauchy family. Sometimes, the structure of the differential equation system yields a solution: For example, Jeffreys (1961) reported a parameter orthogonalization for Pearson’s distributions of type I which is of order $D = 4$. Cox and Reid (1987) further investigate this topic with application to conditional inference, and provide examples (including the Weibull distribution).

From the viewpoint of geometry, the FIM induces a Riemannian manifold with metric tensor $g(\Theta) = \mathcal{I}(\Theta)$. When the FIM may be degenerate, this yields a pseudo-Riemannian manifold (Thomas, 2014). In differential geometry, orthogonalization amounts to transform the square length infinitesimal element $g_{ij} d\Theta_i d\Theta_j$ of a Riemannian geometry into an orthogonal system ω with matching square length infinitesimal element $\Omega_{ii} d\Omega_i d\Omega_j$. However, such a global orthogonal metric does not exist (Huzurbazar, 1950) when $D > 3$ for an arbitrary metric tensor although interesting Riemannian parameterization structures may be derived in Riemannian 4D geometry (Grant and Vickers, 2009). For NEFs, the FIM can be made *block-diagonal* easily by using the *mixed coordinate system* (Amari, 2016) $(\Theta_{1:k}, \mathbf{H}_{k+1:D})$, where $\mathbf{H} = E_p[\mathbf{t}(\mathbf{x})] = \nabla F(\Theta)$ is the moment parameter, for any $k \in \{1, \dots, D-1\}$, where $\mathbf{v}_{[b:e]}$ denotes the subvector $(v_b, \dots, v_e)^T$ of \mathbf{v} . The geometry of NEFs is a dually flat structure (Amari, 2016) induced by the convex mgf, the potential function. It defines a dual affine coordinate systems $e^i = \partial_i = \frac{\partial}{\partial H_i}$ and $e_j = \partial^j = \frac{\partial}{\partial \Theta_j}$ that are orthogonal: $\langle e^i, e_j \rangle = \delta_j^i$, where $\delta_j^i = 1$ iff $i = j$ and $\delta_j^i = 0$ otherwise. Those dual affine coordinate systems are defined up to an affine invertible transformation \mathbf{A} : $\tilde{\Theta} = \mathbf{A}\Theta + \mathbf{b}$, $\tilde{\mathbf{H}} = \mathbf{A}^{-1}\mathbf{H} + \mathbf{c}$, where \mathbf{b} and \mathbf{c} are constants. In particular, for any order-2 NEF ($D = 2$), we can *always* obtain two mixed parameterizations (Θ_1, H_2) or (H_1, Θ_2) .

The FIM $g(\Theta)$ or $\mathcal{I}(\Theta)$ by definition is an expectation. If its Hessian form in eq. (2) is computed based on a set of empirical observations $\{\mathbf{x}_k\}$, as

$$\bar{g}(\Theta) = -\frac{\overline{\partial^2 l_k}}{\partial \Theta_i \partial \Theta_j}, \quad (3)$$

where “ $\overline{\cdot}$ ” denotes the sample average over $\{\mathbf{x}_k\}$, the resulting metric is called the *observed FIM* (Efron and Hinkley, 1978). It is useful when the underlying distribution is not available.

When the number of observations increases, the observed FIM becomes more and more close to the FIM.

Past works on FIM-based approaches mainly focus on how to approximate the global FIM into a block diagonal form using the gradient of the cost function (Roux et al., 2008; Martens, 2010; Pascanu and Bengio, 2014; Martens and Grosse, 2015). This global approach faces the analytical complexity of learning systems. The approximation error increases as the system scales up and as complex and dynamic structures emerge.

This work aims at a different *local* approach. The idea is to *accurately* describe the information geometry in a local subsystem of the big learning system, which is *invariant* to the scaling up and structural change of the global system, so that the local machinery, including optimization, can be discussed regardless of the other parts.

For this purpose, a novel concept, *Relative Fisher Information Metric* (RFIM), is defined. Unlike the traditional geometric view of a high-dimensional parameter manifold, RFIMs defines *multiple projected low-dimensional geometry of subsystems*. This geometry is correlated to the parameters beyond the subsystem and is therefore considered *dynamic*. It can be used to characterize the efficiency of a local learning process. Taking this stance has potentials in deep learning because a big learning system can be decomposed into many local components, i.e. layers. This paper will make clear the concept of RFIM, provide proof-of-concept experiments, and discuss its theoretical advantages.

The paper is organized as follows. Sec. 2 reviews natural gradient within the context of Multi-Layer Perceptrons (MLP). Sec. 3 presents the concept of RFIM, and gives detailed formulations of several commonly used subsystems. Sec. 4 discusses the advantages of using RFIM as compared to FIM. Sec. 5 shows how to use the RFIMs given by Sec. 3 to optimize neural networks, with an algorithm framework and several proof-of-concept experiments. Sec. 6 concludes this work and further hint at perspectives.

2 Natural Gradient of Neural Networks

Consider a MLP as depicted in fig. 1, whose statistical model is the following *conditional distribution*

$$p(\mathbf{y} | \mathbf{x}, \Theta) = \sum_{\mathbf{h}_1, \dots, \mathbf{h}_{L-1}} p(\mathbf{y} | \mathbf{h}_{L-1}, \boldsymbol{\theta}_L) \cdots p(\mathbf{h}_2 | \mathbf{h}_1, \boldsymbol{\theta}_2) p(\mathbf{h}_1 | \mathbf{x}, \boldsymbol{\theta}_1), \quad (4)$$

where the often intractable sum over $\mathbf{h}_1, \dots, \mathbf{h}_{L-1}$ can be get rid off by deteriorating $p(\mathbf{h}_1 | \mathbf{x}, \boldsymbol{\theta}_1), \dots, p(\mathbf{h}_{L-1} | \mathbf{h}_{L-2}, \boldsymbol{\theta}_{L-1})$ to Dirac's deltas δ , and let merely the last layer $p(\mathbf{y} | \mathbf{h}_{L-1}, \boldsymbol{\theta}_L)$ be stochastic. Note that Restricted Boltzmann Machines (Nair and Hinton, 2010; Montavon and Müller, 2012) (RBMs), and dropout (Wager et al., 2013) do consider \mathbf{h} to be stochastic.

The tensor metric of the neuromanifold (Amari, 1995) \mathcal{M}_Θ , consisting of all MLPs with the same architecture but different parameter values, is locally defined by the FIM. Because that a MLP corresponds to a conditional distribution, its FIM by eq. (1) is a function of the input \mathbf{x} . By taking an empirical average over the input samples $\{\mathbf{x}_i\}$, the FIM of a MLP has the following expression

$$g(\Theta) = \frac{1}{n} \sum_{i=1}^n E_{p(\mathbf{y} | \mathbf{x}_i, \Theta)} \left[\frac{\partial l_i}{\partial \Theta} \frac{\partial l_i}{\partial \Theta^\top} \right] = -\frac{1}{n} \sum_{i=1}^n E_{p(\mathbf{y} | \mathbf{x}_i, \Theta)} \left[\frac{\partial^2 l_i}{\partial \Theta \partial \Theta^\top} \right], \quad (5)$$

where $l_i(\Theta) = \ln p(\mathbf{y} | \mathbf{x}_i, \Theta)$ denotes the conditional log-likelihood function wrt \mathbf{x}_i .

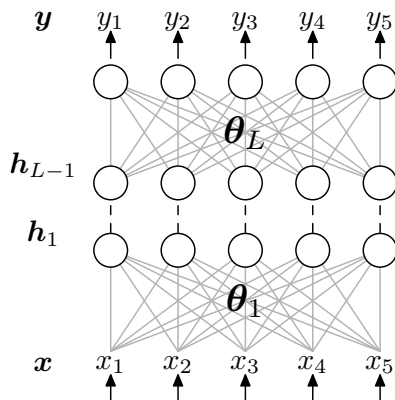


Figure 1: A multilayer perceptron (MLP): A feedforward hierarchical multi-layer machine with hidden layers. The parameter vector $\Theta = (\theta_1, \dots, \theta_L)$ stores the connection weights.

Just like a Mahalanobis metric, $g(\Theta)$ can be used to measure the distance between two neural networks locally around $\Theta \in \mathcal{M}_\Theta$. A learning step makes a tiny movement $\delta\Theta$ on \mathcal{M}_Θ from Θ to $\Theta + \delta\Theta$. According to the FIM, the infinitesimal square distance

$$\langle \delta\Theta, \delta\Theta \rangle_{g(\Theta)} = \delta\Theta^\top g(\Theta) \delta\Theta = \frac{1}{n} \sum_{i=1}^n E_{p(\mathbf{y} | \mathbf{x}_i, \Theta)} \left[\delta\Theta^\top \frac{\partial l_i}{\partial \Theta} \right]^2 \quad (6)$$

measures how much $\delta\Theta$ (with a radius constraint) is statistically along $\frac{\partial l}{\partial \Theta}$, or equivalently how much $\delta\Theta$ affects intrinsically the conditional distribution $p(\mathbf{y} | \mathbf{x}, \Theta)$.

Consider the negative log-likelihood function $L(\Theta) = -\sum_i \ln p(\mathbf{y}_i | \mathbf{x}_i, \Theta)$ wrt the observed pairs $\{(\mathbf{x}_i, \mathbf{y}_i)\}$, we try to minimize the loss while maintaining a small *cost*, measured geometrically by the square distance $\langle \delta\Theta, \delta\Theta \rangle_{g(\Theta)}$ on \mathcal{M}_Θ . At $\Theta_t \in \mathcal{M}_\Theta$, the target is to minimize wrt $\delta\Theta$

$$L(\Theta_t + \delta\Theta) + \frac{1}{2\gamma} \langle \delta\Theta, \delta\Theta \rangle_{g(\Theta_t)} \approx L(\Theta_t) + \delta\Theta^\top \nabla L(\Theta_t) + \frac{1}{2\gamma} \delta\Theta^\top g(\Theta_t) \delta\Theta, \quad (7)$$

where $\gamma > 0$ is a learning rate. The optimal solution of the above eq. (7) gives a learning step

$$\delta\Theta_t = -\gamma g^{-1}(\Theta_t) \nabla L(\Theta_t).$$

In this update procedure, the term $g^{-1}(\Theta_t) \nabla L(\Theta_t)$ replaces the role of the usual gradient $\nabla L(\Theta_t)$ and is called the *natural gradient* (Amari, 1997).

Although the FIM depends on the chosen parameterization, the natural gradient is *invariant* to reparameterization. Let Λ be another coordinate system and \mathbf{J} be the Jacobian matrix $\Theta \rightarrow \Lambda$. Then we have

$$g^{-1}(\Theta) \nabla L(\Theta) = (\mathbf{J}^\top g(\Lambda) \mathbf{J})^{-1} \mathbf{J}^\top \nabla L(\Lambda) = \mathbf{J}^{-1} g^{-1}(\Lambda) \nabla L(\Lambda). \quad (8)$$

The left-hand-side and right-hand-side of eq. (8) correspond to exactly the same infinitesimal movement along \mathcal{M}_Θ . However, as the learning rate γ is not infinitesimal in practice, natural gradient descent actually depends on the coordinate system in practice. Other intriguing properties of natural gradient optimization lie in being free from getting trapped in plateaus of the error surface, and attaining Fisher efficiency in online learning (see Sec. 4 (Amari, 1998)).

For sake of simplicity, we omit to discuss the case when the FIM is singular. That is, the set of parameters Θ_s with zero metric. This set of parameters forms an analytic variety (Watanabe, 2009), and technically the MLP as a statistical model is said non-regular (and the parameter Θ is not identifiable). The natural gradient has been extended (Thomas, 2014) to cope with singular FIMs having positive semi-definite matrices by taking the Moore-Penrose pseudo-inverse (that coincides with the inverse matrix for full rank matrices).

In the family of 2nd-order optimization methods, a line can be drawn from natural gradient from the Newton methods, e.g. (Martens, 2010), by checking whether the computation of the Hessian term depends on the cost function. Taking a MLP as an example, the computation of the FIM does not need the given $\{\mathbf{y}_i\}$, but averages over all possible \mathbf{y} generated according to $\{\mathbf{x}_i\}$ and the current model Θ . One advantage of natural gradient is that the FIM is guaranteed to be psd while the Hessian may not. We refer the reader to related references (Amari et al., 2000) for more details.

Bonnabel (Bonnabel, 2013) proposed to use the Riemannian exponential map to define a step gradient descent, thus ensuring to stay on the manifold for any chosen learning rate. Convergence is proven for Hadamard manifolds (of negative curvatures). However, it is not mathematically tractable to express the exponential map of hierarchical model manifolds.

3 Relative Fisher Information Metric of Subsystems

In general, for large parametric matrices, it is impossible to diagonalize or decorrelate all the parameters as mentioned above, so that we split instead all random variables in the learning system into three parts $\theta_f, \theta, \mathbf{h}$. The *reference*, θ_f , consists of the majority of the random variables that are considered fixed. θ is the internal parameters of a subsystem wrt its structure. The *response* \mathbf{h} is the interface of this subsystem to the rest of the learning system. This \mathbf{h} usually carries sample-wise information to be summarized into the internal parameters θ , so it is like “pseudo-observations”, or hidden variables, to the subsystem. Once θ_f is given, the subsystem can be characterized by the conditional distribution $p(\mathbf{h} | \theta, \theta_f)$. We made the following definition.

Definition 1 (RFIM). *Given θ_f , the RFIM¹ of θ wrt \mathbf{h} is*

$$g^{\mathbf{h}}(\theta | \theta_f) \stackrel{def}{=} E_{p(\mathbf{h} | \theta, \theta_f)} \left[\frac{\partial}{\partial \theta} \ln p(\mathbf{h} | \theta, \theta_f) \frac{\partial}{\partial \theta^T} \ln p(\mathbf{h} | \theta, \theta_f) \right], \quad (9)$$

or simply $g^{\mathbf{h}}(\theta)$, corresponding to the estimation of θ based on observations of \mathbf{h} given θ_f .

When we choose \mathbf{h} to be the observables, usually denoted by \mathbf{x} , and choose θ to be all free parameters Θ in the learning system, then RFIM becomes FIM: $g(\Theta) = g^{\mathbf{x}}(\Theta)$. What is novel is that *we can choose the response \mathbf{h} to be other than the raw observables to compute Fisher informations of subsystems*, specially dynamically during the learning of machines. To see the meaning of RFIM, similar to eq. (6), the infinitesimal square distance

$$\langle \delta \theta, \delta \theta \rangle_{g^{\mathbf{h}}(\theta)} = E_{p(\mathbf{h} | \theta, \theta_f)} \left[\delta \theta^T \frac{\partial}{\partial \theta} \ln p(\mathbf{h} | \theta, \theta_f) \right]^2 \quad (10)$$

measures how much $\delta \theta$ impacts intrinsically the conditional distribution featuring the subsystem. We also have the following proposition, following straightforwardly from definition 1.

¹We use the same term “relative FIM” (Zegers, 2015) with a different definition.

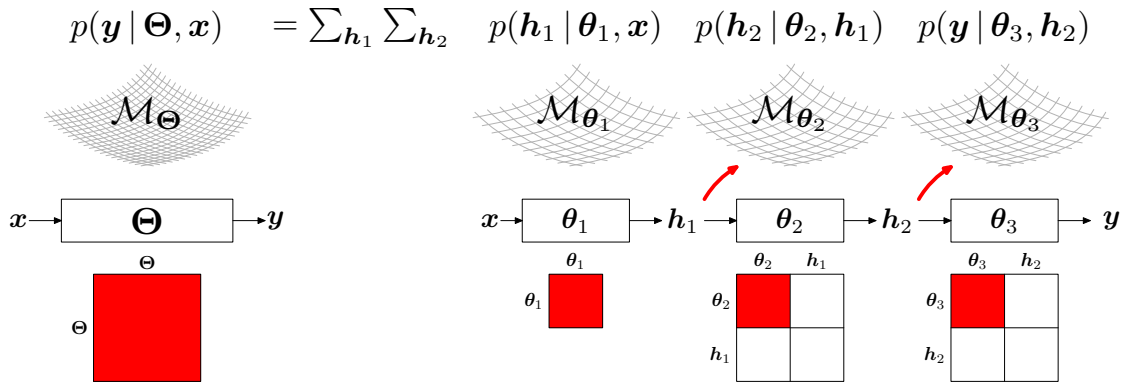


Figure 2: (left) The traditional global geometry of a MLP with two hidden layers; (right) information geometry of subsystems. The red arrows mean that the pointed geometry is *dynamic* wrt to the variable, i.e., the value of the variable affects the geometry. The square under the (sub-)system means the (R-)FIM is computed by (i) computing the FIM in the traditional way wrt all free parameters that affect the system output; (ii) choosing a sub-block as shown by the red square that contains only the internal parameters of the (sub-)system. The rest variables are regarded as the reference.

Proposition 2. *If θ_1 consists of a subset of θ_2 so that $\theta_2 = (\theta_1, \tilde{\theta}_1)$, then \mathcal{M}_{θ_1} with the metric $g^{\mathbf{h}}(\theta_1)$ has the same Riemannian geometry with a sub-manifold of \mathcal{M}_{θ_2} with the metric $g^{\mathbf{h}}(\theta_2)$, when $\tilde{\theta}_1$ is given.*

When the response \mathbf{h} is chosen, then different splits of (θ, θ_f) correspond to the same ambient geometry. In fact, the particular case of a mixed coordinate system (that is not an affine coordinate system) induces in information geometry (Amari, 2016) a dual pair of orthogonal e- and m-orthogonal foliations. Our splits in RFIMs consider non-orthogonal foliations that provide the factorization decompositions of the whole manifold into submanifolds, that are the leaves of the foliation (Amari and Nagaoka, 2000).

Figure 2 shows the traditional global geometry of a learning system, as compared to the information geometry of subsystems defined by RFIMs. The red arrows means that the pointed geometry structure is dynamic and varies with the reference variable. In MLPs, the subsystems, i.e. layers, are supervised. Their reference θ_f also carries sample-wise information.

One should not confuse RFIM with the diagonal blocks of FIM. Both their meaning and expression are different. RFIM is computed by *integrating out* hidden variables, or the output of subsystems. FIM is always computed by integrating out the observables.

In the following we analyze accurately several commonly used RFIMs. Note that, the FIMs of small parametric structures such as single neurons have been studied for a long time (Amari, 1997). Although with similar expressions, we are looking at a component embedded in a large system rather than a small single component system. These are two different concepts, and only the former can be used to guide large learning systems.

3.1 RFIMs of One Neuron

We start from the RFIM of single neuron models.

3.1.1 Hyperbolic tangent activation

Consider a neuron with input \mathbf{x} , weights \mathbf{w} , a hyperbolic tangent activation function, and a stochastic output $y \in \{-1, 1\}$, given by

$$p(y = 1) = \frac{1 + \tanh(\mathbf{w}^\top \tilde{\mathbf{x}})}{2}, \quad \tanh(t) = \frac{\exp(t) - \exp(-t)}{\exp(t) + \exp(-t)}. \quad (11)$$

For convenience, throughout this paper $\tilde{\mathbf{x}} = (\mathbf{x}^\top, 1)^\top$ denotes the augmented vector of \mathbf{x} (homogeneous coordinates) so that $\mathbf{w}^\top \tilde{\mathbf{x}}$ contains a bias term, and a general linear transformation can be written simply as $\mathbf{A}\tilde{\mathbf{x}}$. By definition 1 and some simple analysis², we get

$$g^y(\mathbf{w} | \mathbf{x}) = \nu_{\tanh}(\mathbf{w}, \mathbf{x}) \tilde{\mathbf{x}} \tilde{\mathbf{x}}^\top, \quad \nu_{\tanh}(\mathbf{w}, \mathbf{x}) = 1 - \tanh^2(\mathbf{w}^\top \tilde{\mathbf{x}}). \quad (12)$$

3.1.2 Sigmoid activation

Similarly, the RFIM of a neuron with input \mathbf{x} , weights \mathbf{w} , a sigmoid activation function, and a stochastic binary output $y \in \{0, 1\}$, where

$$p(y = 1) = \text{sigm}(\mathbf{w}^\top \tilde{\mathbf{x}}), \quad \text{sigm}(t) = \frac{1}{1 + \exp(-t)}, \quad (13)$$

is given by

$$\begin{aligned} g^y(\mathbf{w} | \mathbf{x}) &= \nu_{\text{sigm}}(\mathbf{w}, \mathbf{x}) \tilde{\mathbf{x}} \tilde{\mathbf{x}}^\top, \\ \nu_{\text{sigm}}(\mathbf{w}, \mathbf{x}) &= \text{sigm}(\mathbf{w}^\top \tilde{\mathbf{x}}) [1 - \text{sigm}(\mathbf{w}^\top \tilde{\mathbf{x}})]. \end{aligned} \quad (14)$$

A neuron with sigmoid activation but continuous output was discussed earlier (Amari, 1997).

3.1.3 Parametric Rectified Linear Unit

Another commonly used activation function is Parametric Rectified Linear Unit (PReLU) (He et al., 2015), which includes Rectified Linear Unit (ReLU) (Nair and Hinton, 2010) as a special case. To compute the RFIM, we formulate PReLU into a conditional distribution given by

$$p(y | \mathbf{w}, \mathbf{x}) = G(y | \text{relu}(\mathbf{w}^\top \tilde{\mathbf{x}}), \sigma^2), \quad \text{relu}(t) = \begin{cases} t & \text{if } t \geq 0 \\ \iota t & \text{if } t < 0. \end{cases} \quad (0 \leq \iota < 1) \quad (15)$$

When $\iota = 0$, eq. (15) becomes ReLU. By definition 1, the corresponding RFIM is

$$g^y(\mathbf{w} | \mathbf{x}) = \begin{cases} \frac{1}{\sigma^2} \tilde{\mathbf{x}} \tilde{\mathbf{x}}^\top & \text{if } \mathbf{w}^\top \tilde{\mathbf{x}} > 0 \\ \text{undefined} & \text{if } \mathbf{w}^\top \tilde{\mathbf{x}} = 0 \\ \frac{\iota^2}{\sigma^2} \tilde{\mathbf{x}} \tilde{\mathbf{x}}^\top & \text{if } \mathbf{w}^\top \tilde{\mathbf{x}} < 0 \end{cases} \quad (16)$$

This RFIM is discontinuous at $\mathbf{w}^\top \tilde{\mathbf{x}} = 0$. To obtain a smoother RFIM, a trick is to replace $\text{relu}(\mathbf{w}^\top \tilde{\mathbf{x}})$ on the left-hand-side of eq. (15) with $\text{relu}_\omega(\mathbf{w}^\top \tilde{\mathbf{x}})$, where

$$\text{relu}_\omega(t) = \omega \ln \left(\exp \left(\frac{\iota t}{\omega} \right) + \exp \left(\frac{t}{\omega} \right) \right), \quad (17)$$

²See the appendix for detailed derivations.

and $\omega > 0$ is a hyper-parameter so that $\lim_{\omega \rightarrow 0^+} \text{relu}_\omega = \text{relu}$. Then, PReLU's RFIM is given by

$$\begin{aligned} g^y(\mathbf{w} | \mathbf{x}) &= \nu_{\text{relu}}(\mathbf{w}, \mathbf{x}) \tilde{\mathbf{x}} \tilde{\mathbf{x}}^\top, \\ \nu_{\text{relu}}(\mathbf{w}, \mathbf{x}) &= \frac{1}{\sigma^2} \left[\iota + (1 - \iota) \text{sigm} \left(\frac{1 - \iota}{\omega} \mathbf{w}^\top \tilde{\mathbf{x}} \right) \right]^2, \end{aligned} \quad (18)$$

which is simply a smoothed version of eq. (16). If we set empirically $\sigma = 1$, $\iota = 0$, then $\nu_{\text{relu}}(\mathbf{w}, \mathbf{x}) = \text{sigm}^2 \left(\frac{1}{\omega} \mathbf{w}^\top \tilde{\mathbf{x}} \right)$ is close to 1 when $\mathbf{w}^\top \tilde{\mathbf{x}} > 0$, and is close to 0 otherwise.

3.1.4 Exponential Linear Unit

A stochastic exponential linear unit (ELU) (Clevert et al., 2015) with $\alpha > 0$ is

$$p(y | \mathbf{w}, \mathbf{x}) = G(y | \text{elu}(\mathbf{w}^\top \tilde{\mathbf{x}}), \sigma^2), \quad \text{elu}(t) = \begin{cases} t & \text{if } t \geq 0 \\ \alpha (\exp(t) - 1) & \text{if } t < 0. \end{cases} \quad (19)$$

Its RFIM is given by

$$\begin{aligned} g^y(\mathbf{w} | \mathbf{x}) &= \nu_{\text{elu}}(\mathbf{w}, \mathbf{x}) \tilde{\mathbf{x}} \tilde{\mathbf{x}}^\top, \\ \nu_{\text{elu}}(\mathbf{w}, \mathbf{x}) &= \begin{cases} \frac{1}{\sigma^2} & \text{if } \mathbf{w}^\top \tilde{\mathbf{x}} \geq 0 \\ \frac{\alpha^2}{\sigma^2} \exp(2\mathbf{w}^\top \tilde{\mathbf{x}}) & \text{if } \mathbf{w}^\top \tilde{\mathbf{x}} < 0. \end{cases} \end{aligned} \quad (20)$$

The coefficient function $\nu_{\text{elu}}(\mathbf{w}, \mathbf{x})$ is continuous but non-differentiable at $\mathbf{w}^\top \tilde{\mathbf{x}} = 0$.

3.1.5 A generic expression of one-neuron RFIMs

Denote $f \in \{\text{tanh}, \text{sigm}, \text{relu}, \text{elu}\}$ to be an element-wise nonlinear activation function. By eqs. (12), (14) and (18), the RFIMs of single neurons have a common form

$$g^y(\mathbf{w} | \mathbf{x}) = \nu_f(\mathbf{w}, \mathbf{x}) \tilde{\mathbf{x}} \tilde{\mathbf{x}}^\top, \quad (21)$$

where $\nu_f(\mathbf{w}, \mathbf{x})$ is a positive coefficient with large values in the linear region, or the effective learning zone of the neuron.

3.2 RFIM of One Layer

A *linear* layer with input \mathbf{x} , connection weights $\mathbf{W} = [\mathbf{w}_1, \dots, \mathbf{w}_{D_y}]$, and stochastic output \mathbf{y} can be represented by $p(\mathbf{y} | \mathbf{W}, \mathbf{x}) = G(\mathbf{y} | \mathbf{W}^\top \tilde{\mathbf{x}}, \sigma^2 \mathbf{I})$, where \mathbf{I} is the identity matrix, and σ is the scale of the observation noise. We vectorize \mathbf{W} by stacking its columns $\{\mathbf{w}_i\}$, then $g^y(\mathbf{W} | \mathbf{x})$ is a tensor of size $(D_x + 1)D_y \times (D_x + 1)D_y$, where D denotes the dimension of the corresponding variable. Fortunately, due to conditional independence of \mathbf{y} 's dimensions given \mathbf{W} and \mathbf{x} , the RFIM has a simple block diagonal form, given by

$$g^y(\mathbf{W} | \mathbf{x}) = \frac{1}{\sigma^2} \text{diag} [\tilde{\mathbf{x}} \tilde{\mathbf{x}}^\top, \dots, \tilde{\mathbf{x}} \tilde{\mathbf{x}}^\top], \quad (22)$$

where $\text{diag}(\cdot)$ means the (block) diagonal matrix constructed by the given matrix entries.

A *nonlinear* layer increments a linear layer by adding an element-wise activation function applied on $\mathbf{W}^\top \tilde{\mathbf{w}}$, and randomized wrt the choice of the activation (Bernoulli for tanh and sigm ; Gaussian for relu). By definition 1, its RFIM is given by

$$g^y(\mathbf{W} | \mathbf{x}) = \text{diag} [\nu_f(\mathbf{w}_1, \mathbf{x}) \tilde{\mathbf{x}} \tilde{\mathbf{x}}^\top, \dots, \nu_f(\mathbf{w}_m, \mathbf{x}) \tilde{\mathbf{x}} \tilde{\mathbf{x}}^\top], \quad (23)$$

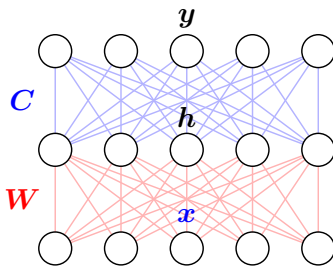


Figure 3: Two layers embedded in a MLP. The red lines and symbols show the interested parameters whose RFIM is to be computed. The blue lines and symbols show the reference variables that is considered given.

where $\nu_f(\mathbf{w}_i, \mathbf{x})$ depends on the activation function f as discussed in Subsec. 3.1.

A softmax layer, which often appears as the last layer of a MLP, is given by $y \in \{1, \dots, m\}$, where

$$p(y) = \eta_y = \frac{\exp(\mathbf{w}_y \tilde{\mathbf{x}})}{\sum_{i=1}^m \exp(\mathbf{w}_i \tilde{\mathbf{x}})}. \quad (24)$$

Its RFIM is not block diagonal any more but given by

$$g^{\mathbf{y}}(\mathbf{W}) = \begin{bmatrix} (\eta_1 - \eta_1^2) \tilde{\mathbf{x}} \tilde{\mathbf{x}}^\top & -\eta_1 \eta_2 \tilde{\mathbf{x}} \tilde{\mathbf{x}}^\top & \cdots & -\eta_1 \eta_m \tilde{\mathbf{x}} \tilde{\mathbf{x}}^\top \\ -\eta_2 \eta_1 \tilde{\mathbf{x}} \tilde{\mathbf{x}}^\top & (\eta_2 - \eta_2^2) \tilde{\mathbf{x}} \tilde{\mathbf{x}}^\top & \cdots & -\eta_2 \eta_m \tilde{\mathbf{x}} \tilde{\mathbf{x}}^\top \\ \vdots & \vdots & \ddots & \vdots \\ -\eta_m \eta_1 \tilde{\mathbf{x}} \tilde{\mathbf{x}}^\top & -\eta_m \eta_2 \tilde{\mathbf{x}} \tilde{\mathbf{x}}^\top & \cdots & (\eta_m - \eta_m^2) \tilde{\mathbf{x}} \tilde{\mathbf{x}}^\top \end{bmatrix}. \quad (25)$$

Notice that its i 'th diagonal block $(\eta_i - \eta_i^2) \tilde{\mathbf{x}} \tilde{\mathbf{x}}^\top$ resembles the RFIM of a single `sigm` neuron.

3.3 RFIM of Two Layers

By eq. (23), the one-layer RFIM is a product metric (Jost, 2011) and does not consider the inter-neuron correlations. We must look at a larger subsystem to obtain such correlations. Consider a two-layer model with stochastic output \mathbf{y} around the mean vector $f(\mathbf{C}^\top \mathbf{h})$, where $\mathbf{h} = f(\mathbf{W}^\top \mathbf{x})$, as shown in fig. 3. For simplicity, we ignore inter-layer correlations between the first layer and the second layer and focus on the inter-neuron correlations within the first layer. To do this, both \mathbf{x} and \mathbf{C} are considered as references to compute the RFIM of \mathbf{W} . By definition 1, $g^{\mathbf{y}}(\mathbf{W} | \mathbf{x}, \mathbf{C}) = [\mathbf{G}_{ij}]_{D_h \times D_h}$ and each block

$$\mathbf{G}_{ij} = \sum_{l=1}^{D_y} c_{il} c_{jl} \nu_f(c_l, \mathbf{h}) \nu_f(\mathbf{w}_i, \mathbf{x}) \nu_f(\mathbf{w}_j, \mathbf{x}) \tilde{\mathbf{x}} \tilde{\mathbf{x}}^\top, \quad \forall 1 \leq i \leq D_h, \quad \forall 1 \leq j \leq D_h. \quad (26)$$

Consider the computational difficulty of eq. (26) that is only listed here as an analytical contribution with possible empirical extensions.

4 Advantages of RFIM

This section discusses theoretical advantages of RFIM. Consider wlog a MLP with one Bernoulli output y , whose mean μ is a deterministic function depending on the input \mathbf{x} and the network

parameters Θ . By Sec. 2, the FIM of the MLP can be computed as

$$g(\Theta) = \mu_i \frac{\partial \ln \mu_i}{\partial \Theta} \frac{\partial \ln \mu_i}{\partial \Theta^\top} + (1 - \mu_i) \frac{\partial \ln(1 - \mu_i)}{\partial \Theta} \frac{\partial \ln(1 - \mu_i)}{\partial \Theta^\top} = \frac{1}{\mu_i(1 - \mu_i)} \frac{\partial \mu_i}{\partial \Theta} \frac{\partial \mu_i}{\partial \Theta^\top}. \quad (27)$$

Therefore $\text{rank}(g(\Theta)) \leq n$, as each sample contributes maximally 1 to the rank of $g(\Theta)$. A small diagonal block of $g(\Theta)$, representing one layer, is likely to have a rank much lower than the sample size. If the number of parameters is greater than the sample size, which can be achieved especially with deep learning (Szegedy et al., 2015), then $g(\Theta)$ is guaranteed to be singular. All methods trying to approximate FIM suffers from this problem and should use proper regularizations. Comparatively, RFIM decomposes the network in a layer-wise manner. In each layer $\mathbf{h} = f(\mathbf{W}^\top \mathbf{x})$, by eq. (23), $\text{rank}(g^{\mathbf{h}}(\mathbf{W})) \leq nD_h$, which is an achievable upper bound. Therefore, RFIM is expected to have a much higher rank than FIM. Higher rank means less singularity, and more information is captured, and easier to reparameterize to achieve good optimization properties. Essentially, RFIM integrates the *internal stochasticity* (Bengio, 2013) of the neural system by considering the output of each layer as random variables. In theory, the computation of FIM should also consider stochastic neurons. However it requires to marginalize the joint distribution of $\mathbf{h}_1, \mathbf{h}_2, \dots, \mathbf{y}$. This makes the already infeasible computation even more difficult.

RFIM is accurate, for that the geometry of θ is defined wrt to its direct response \mathbf{h} in the system, or adjacent nodes in a graphical model. By the example in Sec. 2 and eq. (9), the RFIM $g^{\mathbf{y}}(\theta_L)$ is exactly the corresponding block in the FIM $I(\Theta)$, because they both investigate how θ_L affects the last layer $\mathbf{h}_{L-1} \rightarrow y$. They start to diverge from the second last layer. To compute the geometry of θ_{L-1} , RFIM looks at how θ_{L-1} affects the local mapping $\mathbf{h}_{L-1} \rightarrow \mathbf{h}_L$. Intuitively, this local relationship can be more reliably measured regardless of the rest of the system. In contrast, FIM examines how θ_{L-1} affects the global mapping $\mathbf{h}_{L-1} \rightarrow y$. This task is much more difficult, because it must consider the correlation between different layers. This is hard to perform without approximation techniques. As a commonly used approximation, the block diagonalized version of FIM will ignore such correlations and loose accuracy.

The measurement of RFIM makes it possible to maintain global stability of the learning system by balancing different subsystems. Consider two connected subsystems with internal parameters θ_1 and θ_2 and corresponding responses \mathbf{h}_1 and \mathbf{h}_2 . A learning step is given by $\theta_1 \leftarrow \theta_1 + \delta\theta_1$ and $\theta_2 \leftarrow \theta_2 + \delta\theta_2$, with $\|\delta\theta_1\| \leq \gamma$ and $\|\delta\theta_2\| \leq \gamma$ constrained by a pre-chosen maximum radius γ . To balance the system, we constrain $g^{\mathbf{h}_1}(\theta_1)$ and $g^{\mathbf{h}_2}(\theta_2)$ to have similar scales, e.g. by normalizing their largest eigenvalue to 1. This can be done through reparametrization tricks. Then the intrinsic changes, or variations, of the responses \mathbf{h}_1 and \mathbf{h}_2 also have similar scales and is upper bounded. Note that the responses \mathbf{h}_1 and \mathbf{h}_2 are the interfaces of subsystems. For example, in the MLP shown in fig. 2, the response \mathbf{h}_1 in subsystem 1 becomes the reference in subsystem 2. By bounding the variation of \mathbf{h}_1 , the Riemannian metric $g^{\mathbf{h}_2}(\theta_2 | \mathbf{h}_1)$ will present less variations during learning.

5 Relative Natural Gradient Descent (RNGD)

The traditional non-parametric way of applying natural gradient requires to re-calculate the FIM and solving a large linear system in each learning step. Besides the huge computational cost, it meets some difficulties. For example, in an online learning scenario, a mini batch of samples cannot faithfully reflect the “true” geometry, which has to integrate the risk of sample variations. That is, the FIM of a mini batch is likely to be singular or with bad conditions.

A recent series of efforts (Montavon and Müller, 2012; Raiko et al., 2012; Desjardins et al., 2015) are gearing towards a parametric approach of applying natural gradient, which memorizes

and *learns a geometry*. For example, natural neural networks (Desjardins et al., 2015) augment each layer with a redundant linear layer, and let these linear layers to parametrize the geometry of the neural manifold.

By dividing the learning system into subsystems, RFIM makes this parametric approach much more implementable. The memory complexity of storing the Riemannian metric has been reduced from $O(\#\Theta^2)$ to $O(\sum_i \#\theta_i^2)$, where each θ_i corresponds to a subsystem, and $\#\Theta$ means the dimensionality of Θ . The computational complexity has been reduced from $O(\#\Theta^\rho)$ ($\rho \approx 2.373$, Williams (2012)) to $O(\sum_i \#\theta_i^\rho)$. Approximation techniques of FIM to improve these complexities can be applied to RFIM. Optimization based on RFIM will be called Relative Natural Gradient Descent (RNGD). In the following of this section, we present two examples of RNGD. The objective is to demonstrate its advantages and mechanisms.

5.1 RNGD with a Single `sigm` Neuron

The first experiment is a single neuron model to implement logistic regression (Minka, 2003). The focus of the experiment is to demonstrate the mechanisms of RNGD and to show on a small scale model the improvement made by RNGD over feature whitening techniques, so that we can expect the same improvement on a larger model.

To classify a sample set $\{(\mathbf{x}_i, y_i)\}$ with features \mathbf{x} and class labels $y \in \{0, 1\}$, a statistical model is assumed as

$$\begin{aligned} p(y = 1) &= \text{sigm}(\boldsymbol{\theta}^\top \mathbf{z}), \\ \mathbf{z} &= ((\mathbf{x} - \mathbf{a})^\top \mathbf{A}^\top, 1)^\top. \end{aligned} \quad (28)$$

In eq. (28), $\boldsymbol{\theta}$ is the canonical parameters or the link weights of the neuron. \mathbf{A} and \mathbf{a} are for feature whitening (Montavon and Müller, 2012; Desjardins et al., 2015). They are precomputed and fixed during learning, so that the transformed samples $\{\mathbf{A}(\mathbf{x}_i - \mathbf{a})\}$ have zero mean and unit covariance except singular dimensions. The learning cost function is the average cross entropy

$$L(\boldsymbol{\theta}) = \overline{-y_i \ln \text{sigm}(\boldsymbol{\theta}^\top \mathbf{z}_i) - (1 - y_i) \ln [1 - \text{sigm}(\boldsymbol{\theta}^\top \mathbf{z}_i)]}, \quad (29)$$

whose gradient is simply $\nabla L = \overline{(\text{sigm}(\boldsymbol{\theta}^\top \mathbf{z}_i) - y_i) \mathbf{z}_i}$. To apply RNGD, by eq. (14), we have $g^y(\boldsymbol{\theta}) = \overline{\nu_{\text{sigm}}(\boldsymbol{\theta}, \mathbf{z}_i) \mathbf{z}_i \mathbf{z}_i^\top}$. In each learning step, we update $\boldsymbol{\theta}$ based on

$$\boldsymbol{\theta}^{\text{new}} \leftarrow \boldsymbol{\theta}^{\text{old}} - \gamma(g^y(\boldsymbol{\theta}) + \epsilon \mathbf{I})^{-1} \nabla L, \quad (30)$$

where γ is a learning rate, and $\epsilon > 0$ is a hyper-parameter to guarantee that $(g^y(\boldsymbol{\theta}) + \epsilon \mathbf{I})$ is invertible. We choose empirically ϵ to be $\epsilon \text{tr}(g^y(\boldsymbol{\theta}))/D$, where $\epsilon = 10^{-2}$.

Based on a gradient descent optimizer with constant learning rate and momentum, we compare four different methods:

1. GD fixes $\mathbf{A} = \mathbf{I}$, $\mathbf{a} = \mathbf{0}$, and applies gradient descent;
2. `WhiteGD` performs feature whitening by pre-computing \mathbf{A} and \mathbf{a} as well as gradient descent;
3. NGD fixes $\mathbf{A} = \mathbf{I}$, $\mathbf{a} = \mathbf{0}$, and updates $\boldsymbol{\theta}$ based on eq. (30);
4. `WhiteNGD` performs both feature whitening and the updating scheme in eq. (30).

Based on the MNIST dataset (LeCun et al., 1998), fig. 4 shows their learning curves on binary classification problems “3” vs “5” and “4” vs “9” on two different training sizes. For each method, the best curve which achieved the minimal training error after 100 epochs is shown. The configuration

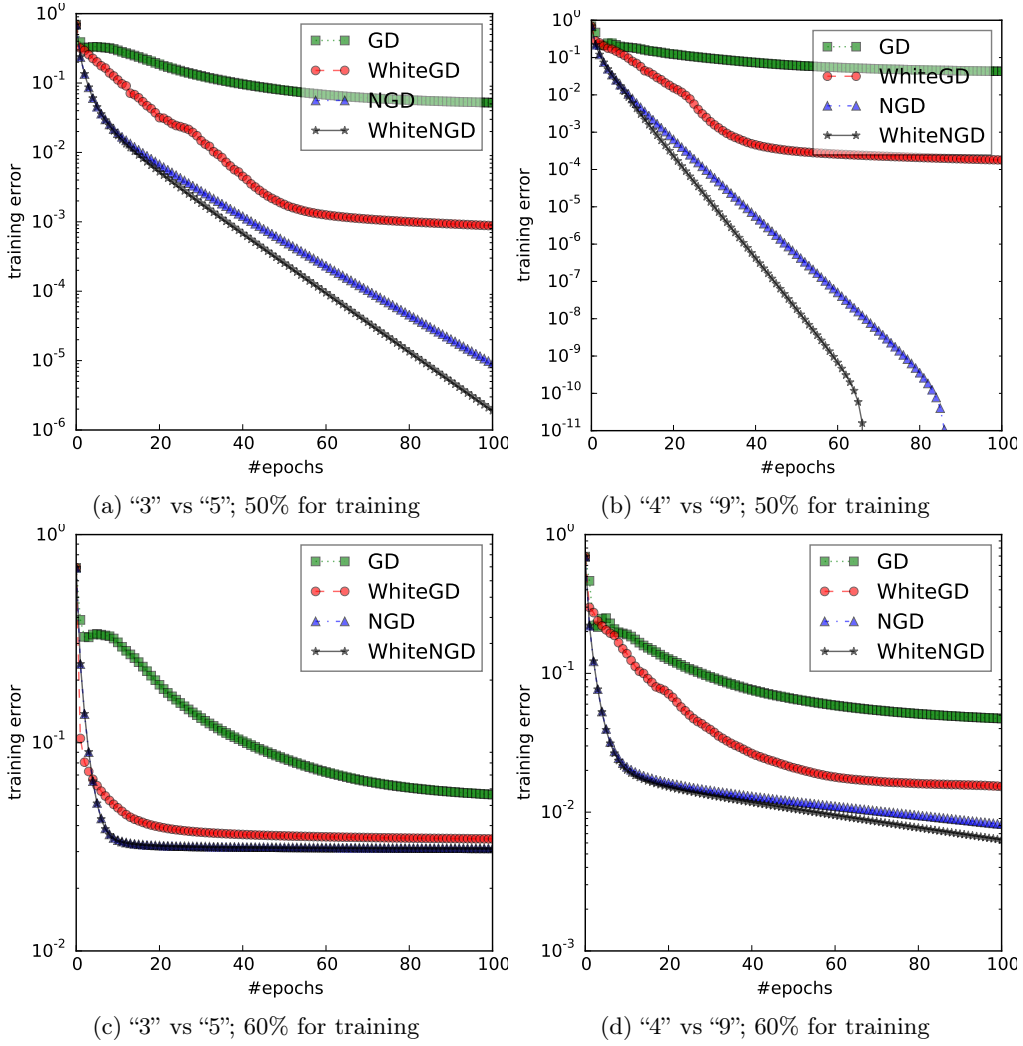


Figure 4: Learning curves of single `sigm` neuron classifiers (better viewed in color). Each curve is an average over ten runs. For each method, the best curve over a configuration grid of learning rates and momentums is presented.

grid is given as follows. The candidate learning rate is in the range $\{10^{-2}, 10^{-1}, 1, 10, 100\}$. The candidate momentum is in the range $\{0, 0.8\}$.

In different cases, `WhiteNGD` and `NGD` can consistently reach deeper in the error surface within a reasonable number of epochs as compared to `WhiteGD` and `GD`. Among all methods, `WhiteNGD` performs best, which demonstrates the dependency of natural gradient and RFIM on the coordinate system. In a whitened coordinate system, RFIM is expected to have better conditions in average, and therefore leading to better optimization. Intuitively, in eq. (14), the term $\nu_{\text{sigm}}(\boldsymbol{\theta}, \boldsymbol{x})$ serves as a “selector”, highlighting a subset of $\{\boldsymbol{x}_i\}$ in the linear region of the perceptron. The updating rule in eq. (30) will zoom in and de-correlate the sample variance in this region, and let the classifier focus on the discriminative samples.

Gradient descent depends much more on the choice of the coordinate system. There is a

significant improvement from GD to **WhiteGD**. A whitened coordinate system allows larger learning rates. In the first several epochs, **WhiteGD** can even learn faster than NGD and **WhiteNGD**, as shown in fig. 4c.

5.2 RNGD with a relu MLP

The good performance of batch normalization (BN) (Ioffe and Szegedy, 2015) can be explained using RFIM. Basically, BN uses an *inter-sample* normalization layer to transform the input of each layer, denoted as \mathbf{x} , to be zero mean and unit variance and thus reduces “internal covariate shift”. In a typical case, above this normalization layer is a linear layer given by $\mathbf{y} = \mathbf{W}^\top \mathbf{x}$. By eq. (22), if \mathbf{x} is normalized, then the diagonal entries of $g^{\mathbf{y}}(\mathbf{W})$ becomes uniform. Therefore the geometry of the parameter manifold is conditioned. In this case, BN helps to condition the RFIM of a linear layer.

This subsection looks at a larger subsystem consisting of a linear layer plus a non-linear activation layer above it, given by $\mathbf{y} = f(\mathbf{W}^\top \mathbf{x})$. By eq. (23), its RFIM is $\text{diag}[\nu_f(\mathbf{w}_1, \mathbf{x}) \tilde{\mathbf{x}} \tilde{\mathbf{x}}^\top, \dots, \nu_f(\mathbf{w}_m, \mathbf{x}) \tilde{\mathbf{x}} \tilde{\mathbf{x}}^\top]$. To perform RNGD, one need to update this layer by

$$\begin{aligned} \mathbf{w}_1^{\text{new}} &\leftarrow \mathbf{w}_1^{\text{old}} - \overline{\nu_f(\mathbf{w}_1, \mathbf{x}_i) \tilde{\mathbf{x}}_i \tilde{\mathbf{x}}_i^\top + \epsilon \mathbf{I}}^{-1} \frac{\partial E}{\partial \mathbf{w}_1}, \\ &\dots \\ \mathbf{w}_m^{\text{new}} &\leftarrow \mathbf{w}_m^{\text{old}} - \overline{\nu_f(\mathbf{w}_m, \mathbf{x}_i) \tilde{\mathbf{x}}_i \tilde{\mathbf{x}}_i^\top + \epsilon \mathbf{I}}^{-1} \frac{\partial E}{\partial \mathbf{w}_m}, \end{aligned} \quad (31)$$

where E is the cost function, and $\epsilon > 0$ is a hyper parameter to avoid singularity. However, this update requires solving many linear subsystems and is too expensive to compute. Moreover, we only have a mini batch which contains not enough information to compute the RFIM. To tackle these difficulties, we maintain an *exponentially moving average* of \mathbf{G}_l , the RFIM of the l 'th neuron in this layer. Initially, \mathbf{G}_l is initialized to identity. At each iteration, it is updated by

$$\mathbf{G}_l^{\text{new}} \leftarrow \lambda \mathbf{G}_l^{\text{old}} + (1 - \lambda) \overline{\nu_f(\mathbf{w}_l, \mathbf{x}_i) \tilde{\mathbf{x}}_i \tilde{\mathbf{x}}_i^\top + \epsilon \mathbf{I}}, \quad (32)$$

where the average is taken over all samples in this mini batch, and λ is a decaying rate. Every T iterations, we recompute \mathbf{G}_l^{-1} based on the most current \mathbf{G}_l , and store the resulting \mathbf{G}_l^{-1} . In the next T iterations, this \mathbf{G}_l^{-1} will remain constant and be used as an approximation of inverse RFIM. Then, the updating rule of the layer is given by

$$\mathbf{w}_1^{\text{new}} \leftarrow \mathbf{w}_1^{\text{old}} - \mathbf{G}_1^{-1} \frac{\partial E}{\partial \mathbf{w}_1} \quad \dots \quad \mathbf{w}_m^{\text{new}} \leftarrow \mathbf{w}_m^{\text{old}} - \mathbf{G}_m^{-1} \frac{\partial E}{\partial \mathbf{w}_m}. \quad (33)$$

For the input layer which scales with the number of input features, and the final soft-max layer, we apply instead the RFIM of the corresponding linear layer for the consideration of the computational efficiency.

We implemented the proposed method using TensorFlow (Abadi et al., 2015) and applied it to classify MNIST digits. The network has shape 784-64-64-64-10, with **relu** activation units, a final soft-max layer, and uses average cross-entropy as the cost function.

Figure 5 shows the learning curves of different methods. **SGD** is stochastic gradient descent. **ADAM** is the Adam optimizer (Kingma and Ba, 2014). **PLAIN** means a plain MLP without batch normalization. **BNA** and **BNB** are two different implementations of BN, depending on whether BN is performed right before (**BNB**) or right after (**BNA**) the activation of the hidden units. They both use a re-scaling parameter to ensure enough flexibility of the parametric structure (Ioffe and Szegedy, 2015). The epsilon parameter of both **BNA** and **BNB** is set to 10^{-3} . For **RNGD**, we

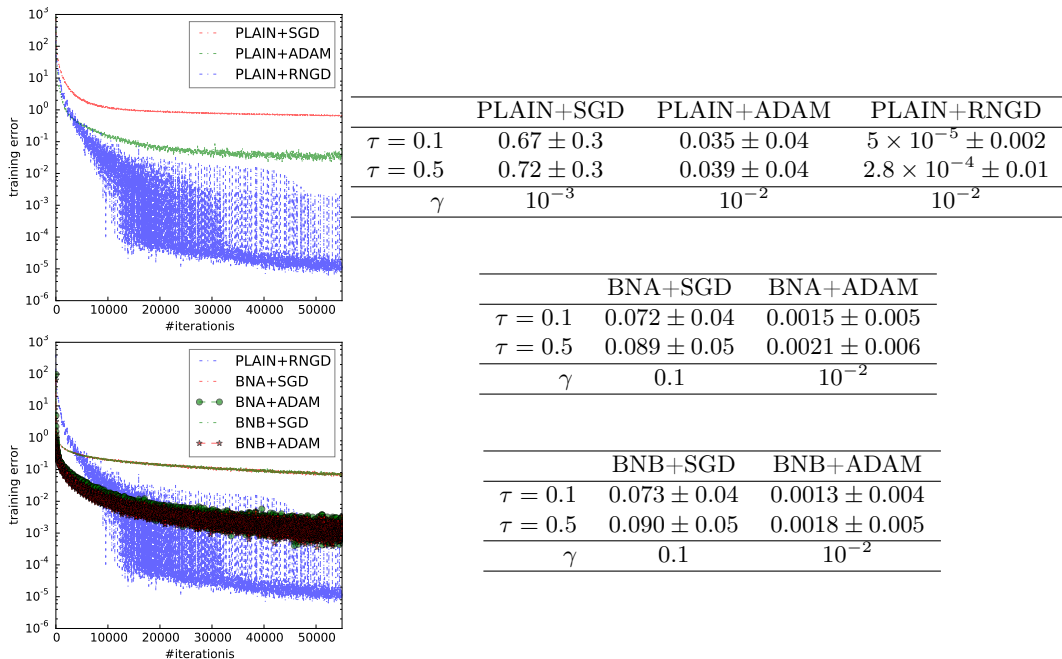


Figure 5: Learning curves on MNIST with `relu` MLPs (better viewed in color). For each method, the best learning curve over several configurations of learning rates is selected. The curves are smoothed by averaging over every 10 iterations for a clear visualization.

set empirically $T = 100$ and $\lambda = 0.995$. The right table shows the mean and standard deviation of the τ -sharp ratio, defined as the training cost over the last τM mini-batch iterations, where $M = 55000$ is the total number of iterations.

We can see that RNGD can significantly improve the learning curve over the other methods and achieve a smaller sharp ratio. The mechanism is similar to the first experiment. By eq. (18), $\nu_{\text{relu}}(\mathbf{w}_i, \mathbf{x})$ is approximately binary, emphasizing such *informative samples* with $\mathbf{w}_i^\top \tilde{\mathbf{x}} > 0$, which are the ones contributing to the learning of \mathbf{w}_i with non-zero gradient values. Each output neuron has a different subset of informative samples. While BN normalizes the layer input \mathbf{x} regardless of the output neurons, RNGD normalizes \mathbf{x} differently wrt different output, so that the informative samples for each output neuron is centered and decorrelated.

As shown in fig. 5, RNGD appears to have a larger variation during learning. This is because of the non-smooth update of the inverse metric. One can however see from the right table that the variation is actually not much, as the y-axis is in log-scale.

By the results of RNGD, it is clear that this MLP structure overfits the input data. It is a fundamental trade-off between fitting the input data and generalizing. This objective of this experiment is mainly focused on improving learning optimization. The overfitting can be tackled by early stopping.

RNGD’s computational time per each iteration is much more than the other methods. In our experiments on a GPU instance of Amazon EC2, RNGD costs around half a minute per each epoch, while the other methods only costs seconds. On CPUs RNGD is even more time consuming. This is both due to the inefficiency of our implementation and its algorithm complexity. To seek efficient RNGD implementations is left for future work.

6 Conclusion and discussion

We propose to investigate local structures of large learning systems using the new concept of Relative Fisher Information Matrix (RFIM). The key advantage of this approach is that the local dynamics can be analyzed in an accurate way without approximation. We present a core list of such local structures in neuron networks, and give their corresponding RFIMs. This list of recipes can be used to provide guiding principles to neuron networks. As a first example, we demonstrated how to apply single neuron RFIM and one layer RFIM to improve the learning curve by using the relative natural gradient descent.

Our work applies to mirror descent as well since natural gradient is related to mirror descent (Raskutti and Mukherjee, 2015) as follows: In mirror descent, given a strictly convex distance function $D(\cdot, \cdot)$ in the first argument (playing the role of the proximity function), we express the gradient descent step as :

$$\Theta_{t+1} = \arg \min_{\Theta} \{ \Theta^\top \nabla F(\Theta_t) + \frac{1}{\gamma} D(\Theta, \Theta_t) \}.$$

When $D(\Theta, \Theta')$ is chosen as a Bregman divergence $B_F((\Theta, \Theta') = F(\Theta) - F(\Theta') - (\Theta - \Theta')^\top \nabla F(\Theta)$, it has been proved that the mirror descent on the Θ -parameterization is equivalent (Raskutti and Mukherjee, 2015) to the natural gradient optimization on the induced Riemannian manifold with metric tensor $(\nabla^2 F(\Theta))$ parameterized by the dual coordinate system $H = \nabla F(\Theta)$. In general, to perform a Riemannian gradient descent for minimizing a real-valued function $f(\Theta)$ on the manifold, one needs to choose a proper metric tensor given in matrix form $G(\Theta)$. Thomas (2014) constructed a toy example showing that the natural gradient may diverge while the ordinary gradient (for $G = I$, the identity matrix) converges. Recently, Thomas et al. (2016) proposed a new kind of descent method based on what they called the Energetic Natural Gradient that generalizes the natural gradient. The energy distance $D_E(p(\Theta_1), p(\Theta_2))^2 = E[2d_{p(\Theta_1)}(X, Y) - d_{p(\Theta_1)}(X, X') - d_{p(\Theta_1)}(Y, Y')]^2$ where $X, X' \sim p(\Theta_1)$ and $Y, Y' \sim p(\Theta_2)$, where $d_{p(\Theta_1)}(\cdot, \cdot)$ is a distance metric over the support. Using a Taylor's expansion on their energy distance, they get the Energy Information Matrix (in a way similar to recovering the FIM from a Taylor's expansion of any f -divergence like the Kullback-Leibler divergence). Their idea is to incorporate prior knowledge on the structure of the support (observation space) to define energy distance. Twisting the geometry of the support (say, Wassertein's optimal transport) with the geometry of the parametric distributions (Fisher-Rao geodesic distances) is indeed important (Chizat et al., 2015). In information geometry, invariance on the support is provided by a Markov morphism that is a probabilistic mapping of support to itself (Čencov, 1982). Markov morphism include deterministic transformation of a random variable by a statistic. It is well-known that $I_T(\Theta) \prec I_X(\Theta)$ with equality iff. $T = T(X)$ is a sufficient statistic of X . Thus to get the same invariance for the energy distance (Thomas et al., 2016), one shall further require $d_{p(\Theta)}(T(X), T(Y)) = d_{p(\Theta)}(X, Y)$.

In the foreseeable future, we believe that Relative Fisher Information Metrics (RFIMs) will provide a sound methodology to build further efficient learning techniques in deep learning.

Our implementation is available at <https://www.lix.polytechnique.fr/~nielsen/RFIM>.

References

- M. Abadi, A. Agarwal, P. Barham, and E. Brevdo. TensorFlow: Large-scale machine learning on heterogeneous systems, 2015. Software available from [tensorflow.org](https://www.tensorflow.org).
- S. Amari. Information geometry of the EM and em algorithms for neural networks. *Neural Networks*, 8(9):1379–1408, 1995.

- S. Amari. Neural learning in structured parameter spaces – natural Riemannian gradient. In *NIPS 9*, pages 127–133. 1997.
- S. Amari. Natural gradient works efficiently in learning. *Neural Comput.*, 10(2):251–276, 1998.
- S. Amari. *Information Geometry and its Applications*, volume 194 of *Applied Mathematical Sciences*. Springer Japan, 2016.
- S. Amari and H. Nagaoka. *Methods of Information Geometry*, volume 191 of *Translations of Mathematical Monographs*. AMS and OUP, 2000. (Published in Japanese in 1993).
- S. Amari, H. Park, and K. Fukumizu. Adaptive method of realizing natural gradient learning for multilayer perceptrons. *Neural Comput.*, 12(6):1399–1409, 2000.
- Y. Bengio. Estimating or propagating gradients through stochastic neurons. *CoRR*, abs/1305.2982, 2013. URL <https://arxiv.org/abs/1305.2982>.
- S. Bonnabel. Stochastic gradient descent on Riemannian manifolds. *IEEE Trans. Automat. Contr.*, 58(9):2217–2229, 2013. doi: 10.1109/TAC.2013.2254619.
- N. N. Čencov. *Statistical decision rules and optimal inference*, volume 53 of *Translations of Mathematical Monographs*. American Mathematical Society, Providence, R.I., 1982. ISBN 0-8218-4502-0. Translation from the Russian edited by Lev J. Leifman.
- L. Chizat, B. Schmitzer, G. Peyré, and F.-X. Vialard. An Interpolating Distance between Optimal Transport and Fisher-Rao. *ArXiv e-prints*, June 2015.
- D. Clevert, T. Unterthiner, and S. Hochreiter. Fast and accurate deep network learning by exponential linear units (elus). *CoRR*, abs/1511.07289, 2015. URL <http://arxiv.org/abs/1511.07289>.
- L. Cobb, P. Koppstein, and N. H. Chen. Estimation and moment recursion relations for multimodal distributions of the exponential family. *JASA*, 78(381):124–130, 1983.
- D. R. Cox and N. Reid. Parameter orthogonality and approximate conditional inference. *Journal of the Royal Statistical Society. Series B (Methodological)*, 49(1):1–39, 1987.
- G. Desjardins, K. Simonyan, R. Pascanu, and K. Kavukcuoglu. Natural neural networks. In *NIPS 28*, pages 2071–2079. 2015.
- B. Efron and D. V. Hinkley. Assessing the accuracy of the maximum likelihood estimator: Observed versus expected Fisher information. *Biometrika*, 65(3):457–487, 1978.
- J. D. Grant and J. Vickers. Block diagonalization of four-dimensional metrics. *Classical and Quantum Gravity*, 26(23):235014, 2009.
- K. He, X. Zhang, S. Ren, and J. Sun. Delving deep into rectifiers: Surpassing human-level performance on ImageNet classification. In *ICCV*, 2015. URL <http://arxiv.org/abs/1502.01852>.
- V. S. Huzurbazar. Probability distributions and orthogonal parameters. In *Mathematical Proceedings of the Cambridge Philosophical Society*, volume 46, pages 281–284. Cambridge Univ Press, 1950.
- S. Ioffe and C. Szegedy. Batch normalization: Accelerating deep network training by reducing internal covariate shift. In *ICML; JMLR: W&CP 37*, pages 448–456, 2015.

- H. Jeffreys. *Theory of Probability*. Oxford University Press, 1961. First published in 1939.
- J. Jost. *Riemannian Geometry and Geometric Analysis*. Springer, 6th edition, 2011.
- D. P. Kingma and J. Ba. Adam: A method for stochastic optimization. *CoRR*, abs/1412.6980, 2014. URL <http://arxiv.org/abs/1412.6980>.
- Y. LeCun, C. Cortes, and C. J. C. Burges. The MNIST database of handwritten digits, 1998. URL <http://yann.lecun.com/exdb/mnist/>.
- J. Martens. Deep learning via Hessian-free optimization. In *ICML*, pages 735–742, 2010.
- J. Martens and R. Grosse. Optimizing neural networks with Kronecker-factored approximate curvature. In *ICML; JMLR: W&CP 37*, pages 2408–2417, 2015.
- T. P. Minka. A comparison of numerical optimizers for logistic regression. Technical report, CMU, 2003. URL <http://research.microsoft.com/en-us/um/people/minka/papers/logreg/>.
- A. Montanari. Computational implications of reducing data to sufficient statistics. *Electron. J. Statist.*, 9(2):2370–2390, 2015.
- G. Montavon and K. R. Müller. Deep Boltzmann machines and the centering trick. In *Neural Networks: Tricks of the Trade*, pages 621–637. 2nd edition, 2012.
- V. Nair and G. E. Hinton. Rectified linear units improve restricted Boltzmann machines. In *ICML*, pages 807–814, 2010.
- R. Pascanu and Y. Bengio. Revisiting natural gradient for deep networks. In *International Conference on Learning Representations*, 2014. URL <http://arxiv.org/abs/1301.3584>.
- T. Raiko, H. Valpola, and Y. LeCun. Deep learning made easier by linear transformations in perceptrons. In *AISTATS; JMLR W&CP 22*, pages 924–932, 2012.
- G. Raskutti and S. Mukherjee. The information geometry of mirror descent. In *Geometric Science of Information - Second International Conference*, volume 9389 of *Lecture Notes in Computer Science*, pages 359–368. Springer, 2015. ISBN 978-3-319-25039-7. doi: 10.1007/978-3-319-25040-3_39. URL <http://dx.doi.org/10.1007/978-3-319-25040-3>.
- N. L. Roux, P. Manzagol, and Y. Bengio. Topmoumoute online natural gradient algorithm. In *NIPS 20*, pages 849–856. 2008.
- C. Szegedy, W. Liu, Y. Jia, P. Sermanet, S. Reed, D. Anguelov, D. Erhan, V. Vanhoucke, and A. Rabinovich. Going deeper with convolutions. In *CVPR*, 2015. URL <http://arxiv.org/abs/1409.4842>.
- P. Thomas. GeNGA: A generalization of natural gradient ascent with positive and negative convergence results. In *Proceedings of the 31st International Conference on Machine Learning (ICML-14)*, pages 1575–1583, 2014.
- P. Thomas, B. C. da Silva, C. Dann, and E. Brunskill. Energetic natural gradient descent. In *Proceedings of the 33rd International Conference on Machine Learning (ICML-16)*, 2016.
- S. Wager, S. Wang, and P. S. Liang. Dropout training as adaptive regularization. In *NIPS 26*, pages 351–359. 2013.

S. Watanabe. *Algebraic Geometry and Statistical Learning Theory*, volume 25 of *Cambridge Monographs on Applied and Computational Mathematics*. Cambridge University Press, 2009.

V. V. Williams. Multiplying matrices faster than coppersmith-Winograd. In *Annual ACM Symposium on Theory of Computing*, STOC'12, pages 887–898, 2012.

P. Zegers. Fisher information properties. *Entropy*, 17:4918–4939, 2015.

A Non-linear Activation Functions

By definition,

$$\tanh(t) \stackrel{def}{=} \frac{\exp(t) - \exp(-t)}{\exp(t) + \exp(-t)}, \quad (34)$$

and

$$\operatorname{sech}(t) \stackrel{def}{=} \frac{2}{\exp(t) + \exp(-t)}. \quad (35)$$

It is easy to verify that

$$\operatorname{sech}^2(t) = [1 + \tanh(t)][1 - \tanh(t)] = 1 - \tanh^2(t). \quad (36)$$

By eq. (34),

$$\begin{aligned} \tanh'(t) &= \frac{\exp(t) + \exp(-t)}{\exp(t) + \exp(-t)} - \frac{\exp(t) - \exp(-t)}{[\exp(t) + \exp(-t)]^2} [\exp(t) - \exp(-t)] \\ &= \frac{[\exp(t) + \exp(-t)]^2 - [\exp(t) - \exp(-t)]^2}{[\exp(t) + \exp(-t)]^2} = \frac{4}{[\exp(t) + \exp(-t)]^2} = \operatorname{sech}^2(t). \end{aligned} \quad (37)$$

By definition,

$$\operatorname{sigm}(t) \stackrel{def}{=} \frac{1}{1 + \exp(-t)}. \quad (38)$$

Therefore

$$\operatorname{sigm}'(t) = -\frac{1}{[1 + \exp(-t)]^2} (-\exp(-t)) = \frac{\exp(-t)}{[1 + \exp(-t)]^2} = \operatorname{sigm}(t) [1 - \operatorname{sigm}(t)]. \quad (39)$$

By definition,

$$\operatorname{relu}_\omega(t) \stackrel{def}{=} \omega \ln \left(\exp \left(\frac{t}{\omega} \right) + \exp \left(\frac{t}{\omega} \right) \right), \quad (40)$$

where $\omega > 0$ and $0 \leq \iota < 1$. Then,

$$\begin{aligned}
\text{relu}'_{\omega}(t) &= \omega \frac{1}{\exp\left(\frac{\iota t}{\omega}\right) + \exp\left(\frac{t}{\omega}\right)} \left(\frac{\iota}{\omega} \exp\left(\frac{\iota t}{\omega}\right) + \frac{1}{\omega} \exp\left(\frac{t}{\omega}\right) \right) \\
&= \frac{\iota \exp\left(\frac{\iota t}{\omega}\right) + \exp\left(\frac{t}{\omega}\right)}{\exp\left(\frac{\iota t}{\omega}\right) + \exp\left(\frac{t}{\omega}\right)} \\
&= \iota + (1 - \iota) \frac{\exp\left(\frac{t}{\omega}\right)}{\exp\left(\frac{\iota t}{\omega}\right) + \exp\left(\frac{t}{\omega}\right)} \\
&= \iota + (1 - \iota) \frac{1}{\exp\left((\iota - 1)\frac{t}{\omega}\right) + 1} \\
&= \iota + (1 - \iota) \text{sigm}\left(\frac{1 - \iota}{\omega} t\right). \tag{41}
\end{aligned}$$

By definition,

$$\text{elu}(t) = \begin{cases} t & \text{if } t \geq 0 \\ \alpha(\exp(t) - 1) & \text{if } t < 0. \end{cases} \tag{42}$$

Therefore

$$\text{elu}'(t) = \begin{cases} 1 & \text{if } t \geq 0 \\ \alpha \exp(t) & \text{if } t < 0. \end{cases} \tag{43}$$

B A Single tanh Neuron

Consider a neuron with parameters \mathbf{w} and a Bernoulli output $y \in \{+, -\}$, $p(y = +) = p^+$, $p(y = -) = p^-$, and $p^+ + p^- = 1$. By the definition of RFIM, we have

$$\begin{aligned}
g^y(\mathbf{w}) &= p^+ \frac{\partial \ln p^+}{\partial \mathbf{w}} \frac{\partial \ln p^+}{\partial \mathbf{w}^\top} + p^- \frac{\partial \ln p^-}{\partial \mathbf{w}} \frac{\partial \ln p^-}{\partial \mathbf{w}^\top} \\
&= \frac{1}{p^+} \frac{\partial p^+}{\partial \mathbf{w}} \frac{\partial p^+}{\partial \mathbf{w}^\top} + \frac{1}{p^-} \frac{\partial p^-}{\partial \mathbf{w}} \frac{\partial p^-}{\partial \mathbf{w}^\top}. \tag{44}
\end{aligned}$$

Since $p^+ + p^- = 1$,

$$\frac{\partial p^+}{\partial \mathbf{w}} + \frac{\partial p^-}{\partial \mathbf{w}} = 0. \tag{45}$$

Therefore, the RFIM of a Bernoulli neuron has the general form

$$g^y(\mathbf{w}) = \left(\frac{1}{p^+} + \frac{1}{p^-} \right) \frac{\partial p^+}{\partial \mathbf{w}} \frac{\partial p^+}{\partial \mathbf{w}^\top} = \frac{1}{p^+ p^-} \frac{\partial p^+}{\partial \mathbf{w}} \frac{\partial p^+}{\partial \mathbf{w}^\top}. \tag{46}$$

A single **tanh** neuron with stochastic output $y \in \{-1, 1\}$ is given by

$$p(y = -1) = \frac{1 - \mu(\mathbf{x})}{2}, \tag{47}$$

$$p(y = 1) = \frac{1 + \mu(\mathbf{x})}{2}, \tag{48}$$

$$\mu(\mathbf{x}) = \text{tanh}(\mathbf{w}^\top \tilde{\mathbf{x}}). \tag{49}$$

By eq. (46),

$$\begin{aligned}
g^y(\mathbf{w}) &= \frac{1}{\frac{1-\mu(\mathbf{x})}{2} \frac{1+\mu(\mathbf{x})}{2}} \left(\frac{1}{2} \frac{\partial \mu}{\partial \mathbf{w}} \right) \left(\frac{1}{2} \frac{\partial \mu}{\partial \mathbf{w}^\top} \right) \\
&= \frac{1}{(1-\mu(\mathbf{x}))(1+\mu(\mathbf{x}))} [1-\mu^2(\mathbf{x})]^2 \tilde{\mathbf{x}} \tilde{\mathbf{x}}^\top \\
&= [1-\mu^2(\mathbf{x})] \tilde{\mathbf{x}} \tilde{\mathbf{x}}^\top \\
&= [1-\tanh^2(\mathbf{w}^\top \tilde{\mathbf{x}})] \tilde{\mathbf{x}} \tilde{\mathbf{x}}^\top \\
&= \operatorname{sech}^2(\mathbf{w}^\top \tilde{\mathbf{x}}) \tilde{\mathbf{x}} \tilde{\mathbf{x}}^\top.
\end{aligned} \tag{50}$$

An alternatively analysis is given as follows. By eqs. (47) to (49),

$$p(y = -1) = \frac{\exp(-\mathbf{w}^\top \tilde{\mathbf{x}})}{\exp(\mathbf{w}^\top \tilde{\mathbf{x}}) + \exp(-\mathbf{w}^\top \tilde{\mathbf{x}})}, \tag{51}$$

$$p(y = 1) = \frac{\exp(\mathbf{w}^\top \tilde{\mathbf{x}})}{\exp(\mathbf{w}^\top \tilde{\mathbf{x}}) + \exp(-\mathbf{w}^\top \tilde{\mathbf{x}})}. \tag{52}$$

Then,

$$\begin{aligned}
g^y(\mathbf{w}) &= E_{y \sim p(y|\mathbf{x})} \left(-\frac{\partial^2 \ln p(y)}{\partial \mathbf{w} \partial \mathbf{w}^\top} \right) \\
&= \frac{\partial^2}{\partial \mathbf{w} \partial \mathbf{w}^\top} \ln [\exp(\mathbf{w}^\top \tilde{\mathbf{x}}) + \exp(-\mathbf{w}^\top \tilde{\mathbf{x}})] \quad (\text{first linear term vanishes}) \\
&= \frac{\partial}{\partial \mathbf{w}^\top} \left[\frac{\exp(\mathbf{w}^\top \tilde{\mathbf{x}}) - \exp(-\mathbf{w}^\top \tilde{\mathbf{x}})}{\exp(\mathbf{w}^\top \tilde{\mathbf{x}}) + \exp(-\mathbf{w}^\top \tilde{\mathbf{x}})} \right] \tilde{\mathbf{x}} \\
&= \frac{\partial}{\partial \mathbf{w}^\top} \tanh(\mathbf{w}^\top \tilde{\mathbf{x}}) \tilde{\mathbf{x}} \\
&= \operatorname{sech}^2(\mathbf{w}^\top \tilde{\mathbf{x}}) \tilde{\mathbf{x}} \tilde{\mathbf{x}}^\top.
\end{aligned} \tag{53}$$

The intuitive meaning of $g^y(\mathbf{w})$ is a weighted covariance to emphasize such “informative” \mathbf{x} ’s that

- are in the linear region of \tanh
- contain “ambiguous” samples

We will need at least $\dim(\mathbf{w})$ samples to make $g^y(\mathbf{w})$ full rank.

C A Single `sigm` Neuron

A single `sigm` neuron is given by

$$p(y = 0) = 1 - \mu(\mathbf{x}), \tag{54}$$

$$p(y = 1) = \mu(\mathbf{x}), \tag{55}$$

$$\mu(\mathbf{x}) = \operatorname{sigm}(\mathbf{w}^\top \tilde{\mathbf{x}}). \tag{56}$$

By eq. (46),

$$\begin{aligned}
g^y(\mathbf{w}) &= \frac{1}{p(y=0)p(y=1)} \frac{\partial p(y=1)}{\partial \mathbf{w}} \frac{\partial p(y=1)}{\partial \mathbf{w}^\top} \\
&= \frac{1}{\mu(\mathbf{x})(1-\mu(\mathbf{x}))} \frac{\partial \mu}{\partial \mathbf{w}} \frac{\partial \mu}{\partial \mathbf{w}^\top} \\
&= \frac{1}{\mu(\mathbf{x})(1-\mu(\mathbf{x}))} \mu^2(\mathbf{x})(1-\mu(\mathbf{x}))^2 \tilde{\mathbf{x}} \tilde{\mathbf{x}}^\top \\
&= \mu(\mathbf{x})(1-\mu(\mathbf{x})) \tilde{\mathbf{x}} \tilde{\mathbf{x}}^\top \\
&= \text{sigm}(\mathbf{w}^\top \tilde{\mathbf{x}}) [1 - \text{sigm}(\mathbf{w}^\top \tilde{\mathbf{x}})] \tilde{\mathbf{x}} \tilde{\mathbf{x}}^\top.
\end{aligned} \tag{57}$$

D A Single relu Neuron

Consider a single neuron with Gaussian output $p(y | \mathbf{w}, \mathbf{x}) = G(y | \mu(\mathbf{w}, \mathbf{x}), \sigma^2)$. Then

$$\begin{aligned}
g^y(\mathbf{w} | \mathbf{x}) &= E_{p(y | \mathbf{w}, \mathbf{x})} \left[\frac{\partial \ln G(y | \mu, \sigma^2)}{\partial \mathbf{w}} \frac{\partial \ln G(y | \mu, \sigma^2)}{\partial \mathbf{w}^\top} \right] \\
&= E_{p(y | \mathbf{w}, \mathbf{x})} \left[\frac{\partial}{\partial \mathbf{w}} \left(-\frac{1}{2\sigma^2} (y - \mu)^2 \right) \frac{\partial}{\partial \mathbf{w}^\top} \left(-\frac{1}{2\sigma^2} (y - \mu)^2 \right) \right] \\
&= E_{p(y | \mathbf{w}, \mathbf{x})} \left[\left(-\frac{1}{\sigma^2} (\mu - y) \right)^2 \frac{\partial \mu}{\partial \mathbf{w}} \frac{\partial \mu}{\partial \mathbf{w}^\top} \right] \\
&= \frac{1}{\sigma^4} E_{p(y | \mathbf{w}, \mathbf{x})} (\mu - y)^2 \frac{\partial \mu}{\partial \mathbf{w}} \frac{\partial \mu}{\partial \mathbf{w}^\top} \\
&= \frac{1}{\sigma^2} \frac{\partial \mu}{\partial \mathbf{w}} \frac{\partial \mu}{\partial \mathbf{w}^\top}.
\end{aligned} \tag{58}$$

A single **relu** neuron is given by

$$\mu(\mathbf{w}, \mathbf{x}) = \text{relu}_\omega(\mathbf{w}^\top \tilde{\mathbf{x}}). \tag{59}$$

By eqs. (41) and (58),

$$g^y(\mathbf{w}) = \frac{1}{\sigma^2} \left[\iota + (1 - \iota) \text{sigm} \left(\frac{1 - \iota}{\omega} \mathbf{w}^\top \tilde{\mathbf{x}} \right) \right]^2 \tilde{\mathbf{x}} \tilde{\mathbf{x}}^\top. \tag{60}$$

E A Single elu Neuron

Similar to the analysis in appendix D, a single **elu** neuron is given by

$$\mu(\mathbf{w}, \mathbf{x}) = \text{elu}(\mathbf{w}^\top \tilde{\mathbf{x}}). \tag{61}$$

By eq. (43),

$$\frac{\partial \mu}{\partial \mathbf{w}} = \begin{cases} \tilde{\mathbf{x}} & \text{if } \mathbf{w}^\top \tilde{\mathbf{x}} \geq 0 \\ \alpha \exp(\mathbf{w}^\top \tilde{\mathbf{x}}) \tilde{\mathbf{x}} & \text{if } \mathbf{w}^\top \tilde{\mathbf{x}} < 0. \end{cases} \tag{62}$$

By eq. (58),

$$g^y(\mathbf{w}) = \begin{cases} \frac{1}{\sigma^2} \tilde{\mathbf{x}} \tilde{\mathbf{x}}^\top & \text{if } \mathbf{w}^\top \tilde{\mathbf{x}} \geq 0 \\ \frac{1}{\sigma^2} (\alpha \exp(\mathbf{w}^\top \tilde{\mathbf{x}}))^2 \tilde{\mathbf{x}} \tilde{\mathbf{x}}^\top & \text{if } \mathbf{w}^\top \tilde{\mathbf{x}} < 0. \end{cases} \tag{63}$$

F RFIM of a Linear Layer

Consider a linear layer

$$p(\mathbf{y}) = G(\mathbf{y} | \mathbf{W}^\top \tilde{\mathbf{x}}, \sigma^2 \mathbf{I}), \quad (64)$$

where $\mathbf{W} = (\mathbf{w}_1, \dots, \mathbf{w}_{D_y})$. By the definition of multivariate Gaussian distribution,

$$\ln p(\mathbf{y}) = -\frac{1}{2} \ln 2\pi - \frac{D_y}{2} \ln \sigma^2 - \frac{1}{2\sigma^2} \sum_{i=1}^{D_y} (y_i - \mathbf{w}_i^\top \tilde{\mathbf{x}})^2. \quad (65)$$

Therefore,

$$\forall i, \quad \frac{\partial}{\partial \mathbf{w}_i} \ln p(\mathbf{y}) = -\frac{1}{\sigma^2} (\mathbf{w}_i^\top \tilde{\mathbf{x}} - y_i) \tilde{\mathbf{x}}. \quad (66)$$

Therefore,

$$\forall i, \forall j \quad \frac{\partial}{\partial \mathbf{w}_i} \ln p(\mathbf{y}) \frac{\partial}{\partial \mathbf{w}_j^\top} \ln p(\mathbf{y}) = \frac{1}{\sigma^4} (y_i - \mathbf{w}_i^\top \tilde{\mathbf{x}}) (y_j - \mathbf{w}_j^\top \tilde{\mathbf{x}}) \tilde{\mathbf{x}} \tilde{\mathbf{x}}^\top. \quad (67)$$

\mathbf{W} is vectorized by stacking its columns $\{\mathbf{w}_i\}_{i=1}^{D_y}$. In the following \mathbf{W} will be used interchangeably to denote either the matrix or its vector form. Correspondingly, the RFIM $g^{\mathbf{y}}(\mathbf{W})$ has $D_y \times D_y$ blocks, where the off-diagonal blocks are

$$\forall i \neq j, \quad E_{p(\mathbf{y})} \left(\frac{\partial}{\partial \mathbf{w}_i} \ln p(\mathbf{y}) \frac{\partial}{\partial \mathbf{w}_j^\top} \ln p(\mathbf{y}) \right) = \frac{1}{\sigma^4} E_{p(\mathbf{y})} [(y_i - \mathbf{w}_i^\top \tilde{\mathbf{x}}) (y_j - \mathbf{w}_j^\top \tilde{\mathbf{x}})] \tilde{\mathbf{x}} \tilde{\mathbf{x}}^\top = \mathbf{0}, \quad (68)$$

and the diagonal blocks are

$$\forall i, \quad E_{p(\mathbf{y})} \left(\frac{\partial}{\partial \mathbf{w}_i} \ln p(\mathbf{y}) \frac{\partial}{\partial \mathbf{w}_i^\top} \ln p(\mathbf{y}) \right) = \frac{1}{\sigma^4} E_{p(\mathbf{y})} (y_i - \mathbf{w}_i^\top \tilde{\mathbf{x}})^2 \tilde{\mathbf{x}} \tilde{\mathbf{x}}^\top = \frac{1}{\sigma^2} \tilde{\mathbf{x}} \tilde{\mathbf{x}}^\top. \quad (69)$$

In summary,

$$g^{\mathbf{y}}(\mathbf{W}) = \frac{1}{\sigma^2} \text{diag}[\tilde{\mathbf{x}} \tilde{\mathbf{x}}^\top, \dots, \tilde{\mathbf{x}} \tilde{\mathbf{x}}^\top]. \quad (70)$$

G RFIM of a Non-Linear Layer

The statistical model of a non-linear layer is

$$p(\mathbf{y} | \mathbf{W}, \mathbf{x}) = \prod_{i=1}^{D_y} p(y_i | \mathbf{w}_i, \mathbf{x}). \quad (71)$$

Then,

$$\ln p(\mathbf{y} | \mathbf{W}, \mathbf{x}) = \sum_{i=1}^{D_y} \ln p(y_i | \mathbf{w}_i, \mathbf{x}). \quad (72)$$

Therefore,

$$\frac{\partial^2}{\partial \mathbf{W} \partial \mathbf{W}^\top} \ln p(\mathbf{y} | \mathbf{W}, \mathbf{x}) = \begin{bmatrix} \frac{\partial^2}{\partial \mathbf{w}_1 \partial \mathbf{w}_1^\top} \ln p(y_1 | \mathbf{w}_1, \mathbf{x}) & & \\ & \ddots & \\ & & \frac{\partial^2}{\partial \mathbf{w}_{D_y} \partial \mathbf{w}_{D_y}^\top} \ln p(y_{D_y} | \mathbf{w}_{D_y}, \mathbf{x}) \end{bmatrix}. \quad (73)$$

Therefore RFIM $g^{\mathbf{y}}(\mathbf{W})$ is a block-diagonal matrix, with the i 'th block given by

$$-E_{p(\mathbf{y}|\mathbf{w},\mathbf{x})} \left[\frac{\partial^2}{\partial \mathbf{w}_i \partial \mathbf{w}_i^\top} \ln p(y_i | \mathbf{w}_i, \mathbf{x}) \right] = -E_{p(y_i | \mathbf{w}_i, \mathbf{x})} \left[\frac{\partial^2}{\partial \mathbf{w}_i \partial \mathbf{w}_i^\top} \ln p(y_i | \mathbf{w}_i, \mathbf{x}) \right], \quad (74)$$

which is simply the single neuron RFIM of the i 'th neuron.

H RFIM of a Softmax Layer

Recall that

$$\forall i \in \{1, \dots, m\}, \quad p(y = i) = \frac{\exp(\mathbf{w}_i \tilde{\mathbf{x}})}{\sum_{i=1}^m \exp(\mathbf{w}_i \tilde{\mathbf{x}})}. \quad (75)$$

Then

$$\forall i, \quad \ln p(y = i) = \mathbf{w}_i \tilde{\mathbf{x}} - \ln \sum_{i=1}^m \exp(\mathbf{w}_i \tilde{\mathbf{x}}). \quad (76)$$

Hence

$$\forall i, \forall j, \quad \frac{\partial \ln p(y = i)}{\partial \mathbf{w}_j} = \delta_{ij} \tilde{\mathbf{x}} - \frac{\exp(\mathbf{w}_j \tilde{\mathbf{x}})}{\sum_{i=1}^m \exp(\mathbf{w}_i \tilde{\mathbf{x}})} \tilde{\mathbf{x}}, \quad (77)$$

where $\delta_{ij} = 1$ if and only if $i = j$ and $\delta_{ij} = 0$ otherwise. Then

$$\begin{aligned} \forall i, \forall j, \forall k, \quad \frac{\partial^2 \ln p(y = i)}{\partial \mathbf{w}_j \partial \mathbf{w}_k^\top} &= -\delta_{jk} \frac{\exp(\mathbf{w}_j \tilde{\mathbf{x}})}{\sum_{i=1}^m \exp(\mathbf{w}_i \tilde{\mathbf{x}})} \tilde{\mathbf{x}} \tilde{\mathbf{x}}^\top + \frac{\exp(\mathbf{w}_j \tilde{\mathbf{x}})}{(\sum_{i=1}^m \exp(\mathbf{w}_i \tilde{\mathbf{x}}))^2} \exp(\mathbf{w}_k \tilde{\mathbf{x}}) \tilde{\mathbf{x}} \tilde{\mathbf{x}}^\top \\ &= (-\delta_{jk} \eta_j + \eta_j \eta_k) \tilde{\mathbf{x}} \tilde{\mathbf{x}}^\top. \end{aligned} \quad (78)$$

The right-hand-side of eq. (78) does not depend on i . Therefore

$$g^{\mathbf{y}}(\mathbf{W}) = \begin{bmatrix} (\eta_1 - \eta_1^2) \tilde{\mathbf{x}} \tilde{\mathbf{x}}^\top & -\eta_1 \eta_2 \tilde{\mathbf{x}} \tilde{\mathbf{x}}^\top & \cdots & -\eta_1 \eta_m \tilde{\mathbf{x}} \tilde{\mathbf{x}}^\top \\ -\eta_2 \eta_1 \tilde{\mathbf{x}} \tilde{\mathbf{x}}^\top & (\eta_2 - \eta_2^2) \tilde{\mathbf{x}} \tilde{\mathbf{x}}^\top & \cdots & -\eta_2 \eta_m \tilde{\mathbf{x}} \tilde{\mathbf{x}}^\top \\ \vdots & \vdots & \ddots & \vdots \\ -\eta_m \eta_1 \tilde{\mathbf{x}} \tilde{\mathbf{x}}^\top & -\eta_m \eta_2 \tilde{\mathbf{x}} \tilde{\mathbf{x}}^\top & \cdots & (\eta_m - \eta_m^2) \tilde{\mathbf{x}} \tilde{\mathbf{x}}^\top \end{bmatrix}. \quad (79)$$

I RFIM of Two layers

Consider a two layer structure, where the output \mathbf{y} satisfies a multivariate Bernoulli distribution with independent dimensions. By a similar analysis to appendix B, we have

$$g^{\mathbf{y}}(\mathbf{W}) = \sum_{l=1}^{D_y} \nu_f(c_l, \mathbf{h}) \frac{\partial \mathbf{c}_l^\top \mathbf{h}}{\partial \mathbf{W}} \frac{\partial \mathbf{c}_l^\top \mathbf{h}}{\partial \mathbf{W}^\top}. \quad (80)$$

It can be written block by block as $g^{\mathbf{y}}(\mathbf{W}) = [\mathbf{G}_{ij}]_{D_h \times D_h}$, where each block \mathbf{G}_{ij} means the correlation between the i 'th hidden neuron with weights \mathbf{w}_i and the j 'th hidden neuron with

weights \mathbf{w}_j . By eq. (80),

$$\begin{aligned}
\mathbf{G}_{ij} &= \sum_{l=1}^{D_y} \nu_f(\mathbf{c}_l, \mathbf{h}) \frac{\partial \mathbf{c}_l^\top \mathbf{h}}{\partial \mathbf{w}_i} \frac{\partial \mathbf{c}_l^\top \mathbf{h}}{\partial \mathbf{w}_j^\top} = \sum_{l=1}^{D_y} \nu_f(\mathbf{c}_l, \mathbf{h}) \frac{\partial c_{il} h_i}{\partial \mathbf{w}_i} \frac{\partial c_{jl} h_j}{\partial \mathbf{w}_j^\top} \\
&= \sum_{l=1}^{D_y} \nu_f(\mathbf{c}_l, \mathbf{h}) c_{il} c_{jl} \frac{\partial h_i}{\partial \mathbf{w}_i} \frac{\partial h_j}{\partial \mathbf{w}_j^\top} = \sum_{l=1}^{D_y} \nu_f(\mathbf{c}_l, \mathbf{h}) c_{il} c_{jl} (\nu_f(\mathbf{w}_i, \mathbf{x}) \tilde{\mathbf{x}}) (\nu_f(\mathbf{w}_j, \mathbf{x}) \tilde{\mathbf{x}}^\top) \\
&= \sum_{l=1}^{D_y} c_{il} c_{jl} \nu_f(\mathbf{c}_l, \mathbf{h}) \nu_f(\mathbf{w}_i, \mathbf{x}) \nu_f(\mathbf{w}_j, \mathbf{x}) \tilde{\mathbf{x}} \tilde{\mathbf{x}}^\top. \tag{81}
\end{aligned}$$

The proof of the other case, where two `relu` layers have stochastic output \mathbf{y} satisfying a multivariate Gaussian distribution with independent dimensions, is very similar and is omitted.